RSC Advances

PAPER

View Article Online
View Journal | View Issue

Cite this: *RSC Adv.*, 2021, **11**, 18840

Synthesis, structures, and catalytic efficiency in ring opening polymerization of *rac*-lactide with tridentate *vs.* bidentate cobalt(II), zinc(II), and cadmium(II) complexes containing *N*-substituted *N*,*N*-bis((3,5-dimethyl-1*H*-pyrazol-1-yl)methyl) amine ligands†

Solhye Choe, [a] Hyosun Lee *[a] and Saira Nayab*[b]

A series of Co(II), Zn(II), and Cd(II) complexes supported by 1-(3,5-dimethyl-1*H*-pyrazol-1-yl)-*N*-((3,5-dimethyl-1*H*-pyrazol-1-yl)methyl)-*N*-(furan-2-ylmethyl)methanamine (L_A) and *N*,*N*-bis((3,5-dimethyl-1*H*-pyrazol-1-yl)methyl)-4-isopropylaniline (L_B) were synthesized. The direct chelation of $CoCl_2 \cdot 6H_2O$, $ZnCl_2$, and $CdBr_2 \cdot 4H_2O$ by the ligands produced **[L_nMX_2]** ($L_n = L_A$ or L_B; M = Zn or Co, with X = Cl; M = Cd, with X = Br) complexes in high yields. Structural studies revealed that **[L_BCoCl_2]** and **[L_BZnCl_2]** adopted distorted tetrahedral geometries, as L_B coordinated the metal centers in a bidentate fashion, while L_A coordinated the metal centers in a tridentate fashion through the nitrogen atoms of the pyrazole and amine moieties, so that **[L_ACoCl_2]** and **[L_AZnCl_2]** exhibited trigonal bipyramidal geometries and **[L_ACdBr_2]** a square pyramidal geometry. **[L_BCdBr_2]** has two Cd-containing structures per unit cell, whereby one Cd center adopted a distorted tetrahedral geometry and the other exhibited square bipyramidal geometry. The *in situ*-generated alkyl derivatives of the synthesized complexes were assessed in the ring-opening polymerization of *rac*-lactide. Heterotactic polylactides (PLAs) were furnished with all complexes. The **[L_BZnCl_2]/MeLi** system produced PLA with a superior heterotactic bias (P_r up to 0.94) at −25 °C. PLAs with wide-ranging polydispersity indices (1.16–2.23) and low molecular weights were produced in all cases, irrespective of the specific M(II) center and ancillary ligand utilized.

Received 25th March 2021
Accepted 20th May 2021

DOI: 10.1039/d1ra02365a

rsc.li/rsc-advances

1. Introduction

Biodegradable polymers have been developed as excellent substitutes for conventional petroleum-based polymers.[1,2] Aliphatic polyesters like polylactide (PLA) are regarded as the most promising candidates to fulfil the described role.[3,4] PLA has garnered particular interest owing to its biocompatibility and biodegradability, and the possibility of producing its component monomers starting from renewable resources.[5,6] Well-defined PLAs with controlled physical and mechanical properties have been employed in a vast range of applications, including packaging, medical implants, tissue engineering, and pharmacology.[7–10] In the recent past, numerous metal complexes, including complexes of Al,[11–15] Zn,[16,17] Ga,[18] In,[19] Cu,[20,21] Co,[22,23] and trivalent rare earths,[24] have been utilized as catalysts for the ring-opening polymerization (ROP) of lactide (LA); notably, such catalysts afforded excellent control over reaction initiation and propagation, as well as the stereochemical arrangement of the polymer chains.[25]

The architecture of the ligand coordinating the metal center is one of the key factors determining the catalyst's ability to control the stereochemistry and properties of the resultant polymer,[26,27] alongside the identity of the metal center and the temperature at which the polymerization reaction is conducted. The prevalent ligand architectures, including diketiminate,[28,29] Schiff bases,[30,31] bis(phenolate),[32,33] salen,[34–36] iminomethylpyridines,[37] (benzoimidazolylmethyl)amine,[38] and (pyrazolylmethyl)pyridine/amine,[39–41] have been widely modified to control their stereo-electronic properties, which in turn affect the activity and stereoselectivity of ROP initiators. Thus, choosing carefully the architecture of the ligand is a *N*-

[a]*Department of Chemistry and Green-Nano Materials Research Center, Kyungpook National University, 80 Daehakro, Bukgu, Daegu, 41566, Republic of Korea. E-mail: hyosunlee@knu.ac.kr; Fax: +82-53-950-6330; Tel: +82-53-950-5337*

[b]*Department of Chemistry, Shaheed Benazir Bhutto University, Sheringal Dir (U), Khyber Pakhtunkhwa, Islamic Republic of Pakistan. E-mail: drnayab@sbbu.edu.pk; sairanayab07@yahoo.com*

† Electronic supplementary information (ESI) available: Scheme, ^{1}H NMR, ^{13}C NMR, FTIR, EA, homodecoupled ^{1}H NMR, GPC, ball and stick model, crystal data and structure refinement, general experimental procedures. CCDC 2068377–2068382 contains the supplementary crystallographic data for **[L_ACoCl_2]**, **[L_AZnCl_2]**, **[L_ACdBr_2]**, **[L_BCoCl_2]**, **[L_BZnCl_2]**, and **[L_BCdBr_2]**, respectively. For ESI and crystallographic data in CIF or other electronic format see DOI: 10.1039/d1ra02365a

substituted bis(pyrazolyl)amine have been attracting particular interest as nitrogen donor ligands, because the pyrazole nitrogen is a weaker δ-donor than imine and pyridine nitrogens, and it affords complexes comprising highly electrophilic M(II) centers.[42] Additionally, the fact that it is possible to modify the linker units comprising two or three pyrazole moieties[43,44] renders various bidentate, tridentate or/and polydentate coordination geometries and nuclearities achievable,[45] and it has been shown to allow the overall adjustment of the steric and electrophilic properties of the resultant metal complexes.[46,47] For instance, the Yu group reported the synthesis of pyrazole-based Zn(II) complexes that proved to be effective ROP catalysts; in fact, they afforded the polymerization of 100 equivalents of *rac*-LA within 1–3 min in the presence of [BeOH] at 25 °C; nevertheless, their use resulted in a negligible stereoregularity of the resultant PLA.[42] Similarly, Kang studied the ability of *in situ*-generated (bdmppea)$ZnEt_2$ (bdmppea: *N*,*N*-bis[(3,5-dimethyl-1*H*-pyrazol-1-yl)methyl]-1-phenylethylamine; Et: ethyl) to catalyze the polymerization of *rac*-LA; the relevant reaction afforded 91% *rac*-LA conversion within 2 h, and it led to the production of moderately heterotactic PLA.[48] In a recently published study conducted by our group, we focused on developing late transition metal complexes based on *N*,*N*-bis((1*H*-pyrazol-1-yl)methyl)amine derivatives with various amine substituents, and we studied their catalytic performances in the ROP of *rac*-LA.[49] The catalytic capabilities of these complexes and the stereoselectivity they afforded were promising, and the relevant reactions yielded PLAs of moderate-to-high molecular weight.[50,51] In the present contribution, we intended to study the catalytic properties of *N*-substituted *N*,*N*-bis((3,5-dimethyl-1*H*-pyrazol-1-yl)methyl)amine-based Zn(II), Co(II), and Cd(II) complexes in the ROP of *rac*-LA.

2. Experimental

2.1. General considerations

The syntheses of ligands 1-(3,5-dimethyl-1*H*-pyrazol-1-yl)-*N*-((3,5-dimethyl-1*H*-pyrazol-1-yl)methyl)-*N*-(furan-2-ylmethyl) methanamine (L_A), and *N*,*N*-bis((3,5-dimethyl-1*H*-pyrazol-1-yl) methyl)-4-isopropylaniline (L_B) and their corresponding M(II) (M = Co, Zn, and Cd) complexes were carried out employing benchtop techniques. The ROP reactions were conducted using a high-vacuum Schlenk line and glove box. The starting materials, including $CoCl_2\cdot 6H_2O$, $ZnCl_2$, $CdBr_2\cdot 4H_2O$, furfurylamine, 4-isopropylanilie, magnesium sulfate ($MgSO_4$), and molecular sieves (0.4 nm), were purchased from Aldrich. Anhydrous solvents, such as ethanol (EtOH), *n*-hexane, and diethyl ether (Et_2O), were purchased from Merck and used without further purification. THF was dried over benzophenone ketyl radical whereas CH_2Cl_2 was dried over CaH_2, and these solvents were deoxygenated by distillation under argon before use. 3,5-Dimethyl-1*H*-pyrazolyl-1-methanol was prepared as reported previously.[52] Notably, the ligands employed in the current study, L_A[53] and L_B,[54] and complex $[L_ACdBr_2]$[51] were synthesized according to previously reported methods. It is important to note that safety protocol should be followed using cadmium bromide salt ($CdBr_2\cdot 4H_2O$) for synthesis of Cd-complexes as they are highly toxic and mishandling can cause skin and respiratory irritation.

The ^{1}H NMR (500 MHz) and ^{13}C NMR (125 MHz) spectra of L_A and L_B (Fig. S1 and S2,† respectively) and their Zn(II) and Cd(II) complexes (Fig. S3–S9†) were recorded on a Bruker Avance Digital NMR spectrometer. Chemical shifts are reported in ppm relative to tetramethylsilane ($SiMe_4$) used as internal standard. Coupling constants are reported in Hertz (Hz). Resonance peaks are reported as m = multiplet, br = broad, s = singlet, d = doublet, t = triplet, and q = quartet. The infrared (IR) spectra of ligands and complexes were recorded on a Bruker FT/IR-Alpha (neat) instrument, and data were reported in wavenumbers (cm^{-1}) (Fig. S10–S17†). Elemental analyses of the synthesized complexes were performed on an elemental analyzer (EA 1108; Carlo-Erba, Milan, Italy) (Fig. S18†). The monomer conversion to PLA was determined by integrating monomer *versus* polymer methine resonances in ^{1}H NMR spectrum of PLAs (Fig. S19–S30†). The microstructure analysis of PLAs was performed by inspecting the methine proton region of homodecoupled ^{1}H NMR spectra of the purified polymers (Fig. S31–S44†).[55–58] The number average molecular weight (M_n) and molecular weight (M_w) values for the purified PLA samples were determined using a Waters Alliance e2695 instrument possessing differential refractive index detectors; this instrument was calibrated against a polystyrene standard. The Water Styragel columns; HR3, HR4, and HR5E, were employed, and THF was utilized as the eluting solvent at a flow rate of 1.0 mL min^{-1} at 35 °C. The polydispersity index (PDI) and M_n values of the polymers were reported with respect to the polystyrene standard (Fig. S45–S58†).

2.2. Synthetic procedures

2.2.1. 1-(3,5-Dimethyl-1*H*-pyrazol-1-yl)-*N*-((3,5-dimethyl-1*H*-pyrazol-1-yl)methyl)-*N*-(furan-2-ylmethyl)methanamine cobalt(II) chloride, [LACoCl2]. A solution of L_A (0.627 g, 2.00 mmol) in anhydrous EtOH (10.0 mL) was added to a solution of $CoCl_2\cdot 6H_2O$ (0.476 g, 2.00 mmol) in anhydrous EtOH (10.0 mL) and stirred at room temperature for 12 h to form a blue powder. The solid was filtered and washed with cold EtOH (20.0 mL × 2), followed by washing with Et_2O (20.0 mL × 3). The product was dried under vacuum to yield final product (0.835 g, 94%). Single crystals suitable for an X-ray diffraction analysis were grown by layering a CH_2Cl_2 solution of $[L_ACoCl_2]$ with *n*-hexane. Analysis calculated for $C_{17}H_{23}Cl_2N_5OCo$ (%): C, 46.15, H, 5.24, N, 15.84. Found: C, 46.29, H, 5.29, N, 15.80. IR (solid neat; cm^{-1}): ν(C–H) 2920 w; ν(C=C) 1549 s; ν(C=C) + ν(C=N)/pz ring, 1493 s, 1463 m; ν_{bend}(C–H sp^3) 1426 m; ν(N–C) 1248 s; ν(C–O) 1151 (s); ν_{bend}(C–H sp^2) 834 w; ν(N–M) 599 w.

2.2.2. 1-(3,5-Dimethyl-1*H*-pyrazol-1-yl)-*N*-((3,5-dimethyl-1*H*-pyrazol-1-yl)methyl)-*N*-(furan-2-ylmethyl)methanamine zinc(II) chloride, [LAZnCl$_2$]. A method analogous to that used to prepare $[L_ACoCl_2]$ was adopted for the synthesis of $[L_AZnCl_2]$; in this case L_A (0.627 g, 2.00 mmol) and $ZnCl_2$ (0.273 g, 2.00 mmol) were used to obtain white powder as a final product (0.827 g, 92%). Single crystals suitable for an X-ray diffraction analysis were grown by layering a CH_2Cl_2 solution of $[L_AZnCl_2]$ with *n*-hexane. ^{1}H NMR ($CDCl_3$, 500 MHz): δ 7.45 (d, 1H, J = 2.75 Hz,

–O–C**H**=CH–CH=C–), 6.41 (dd, 1H, J = 1.84 Hz, 1.83 Hz, –O–CH=C**H**–CH=C–), 6.30 (d, 1H, J = 3.81 Hz, –O–CH=CH–C**H**=C–), 6.04 (s, 2H, –N–C(CH_3)=C**H**–C(CH_3) =N–), 5.02 (s, 4H, –N–C**H**$_2$–N–), 3.72 (s, 2H, –C–CH_2–N–), 2.66 (s, 6H, –N–C(C**H**$_3$)=CH–C(CH_3)=N–), 2.20 (s, 6H, –N–C(CH_3)=CH–C(C**H**$_3$)=N–). ^{13}C NMR (DMSO-d_6, 125 MHz): d 150.61 (s, 1C, –O–CH=CH–CH=**C**–), 147.83 (s, 2C, –N–C(CH_3)=CH–**C**(CH_3)=N–), 143.95 (d, 1C, J = 203.4 Hz, –O–**C**H=CH–CH=C–), 140.94 (s, 2C, –N–**C**(CH_3)=CH–C(CH_3)=N–), 111.46 (d, 1C, J = 192.6 Hz, –O–CH=**C**H–CH=C–), 111.33 (d, 1C, J = 174.4 Hz, –O–CH=CH–**C**H=C–), 107.18 (d, 2C, J = 174.4 Hz, –N–C(CH_3)=**C**H–C(CH_3)=N–), 64.06 (t, 2C, J = 301.5 Hz, –N–**C**H_2–N–), 46.70 (t, 1C, J = 278.8 Hz, –C–CH_2–N–), 15.08 (q, 2C, J = 381.47 Hz, –N–C(**C**H_3)=CH–C(CH_3)=N–), 12.04 (q, 2C, J = 386.0 Hz, –N–C(CH_3)=CH–C(**C**H_3)=N–). Analysis calculated for $C_{17}H_{23}Cl_2N_5OZn$ (%): C, 45.63, H, 5.19, N, 15.66. Found: C, 45.63, H, 5.24, N, 15.92. FTIR (solid neat; cm^{-1}): ν(C–H) 2956 w; ν(C=C) 1610 s; ν(C=C) + ν(C=N)/pz ring, 1514 s, 1458 s; ν_{bend}(C–H sp^3) 1417 m; ν(N–C) 1214 s; ν(C–O) 1120 (s); ν_{bend}(C–H sp^2) 832 w; ν(N–M) 571 w.

2.2.3. *N*,*N*-Bis((3,5-dimethyl-1*H*-pyrazol-1-yl)methyl)-4-isopropylaniline cobalt(II) chloride, [LBCoCl$_2$]. A method analogous to that used to prepare **[L$_A$CoCl$_2$]** was adopted for the synthesis of **[L$_B$CoCl$_2$]**; in this case L$_B$ (0.703 g, 2.00 mmol) and $CoCl_2 \cdot 6H_2O$ (0.476 g, 2.00 mmol) to get blue solid as a final product (0.896 g, 92%). Single crystals suitable for an X-ray diffraction analysis were grown by layering a CH_2Cl_2 solution of **[L$_B$CoCl$_2$]** with *n*-hexane. Analysis calculated for $C_{21}H_{29}Cl_2N_5Co$ (%): C, 52.49, H, 6.09, N, 14.58. Found: C, 52.61, H, 6.06, N, 14.24. FTIR (solid neat; cm^{-1}): ν(C–H) 2952 w; ν(C=C) 1608 s; ν(C=C) + ν(C=N)/pz ring, 1512 s, 1460 s; ν_{bend}(–C–H sp^3) 1414 m; ν(N–C) 1210 s; ν_{bend}(C–H sp^2) 831 w; ν(N–M) 570 w.

2.2.4. *N*,*N*-Bis((3,5-dimethyl-1*H*-pyrazol-1-yl)methyl)-4-isopropylaniline zinc(II) chloride [L$_B$ZnCl$_2$]. A method analogous to that used to prepare **[L$_A$CoCl$_2$]** was adopted for the synthesis of **[L$_B$ZnCl$_2$]**; in this case L$_B$ (0.703 g, 2.00 mmol) and $ZnCl_2$ (0.273 g, 2.00 mmol) were used to get white solid as a final product (0.815 g, 83%). Single crystals suitable for an X-ray diffraction analysis were grown by layering a CH_2Cl_2 solution of **[L$_B$ZnCl$_2$]** with *n*-hexane. Analysis calculated for $C_{21}H_{29}Cl_2N_5Zn$ (%): C, 51.95, H, 6.02, N, 14.43. Found: C, 51.72, H, 6.00, N, 14.78. ^{1}H NMR ($CDCl_3$, 500 MHz): δ 7.22 (d, 2H, J = 8.24 Hz, –C$_6$**H**$_4$–), 6.82 (d, 2H, J = 8.54 Hz, –C$_6$**H**$_4$–), 6.00 (s, 2H, –N–C(CH_3)=C**H**–C(CH_3)=N–), 5.35 (s, 4H, –N–C**H**$_2$–N–), 2.95–2.90 (m, 1H, J = 27.62 Hz, iso-C$_3$**H**$_7$–), 2.72 (s, 6H, –N–C(CH_3)=CH–C(C**H**$_3$)=N–), 1.83 (s, 6H, –N–C(C**H**$_3$)=CH–C(CH_3)=N–), 1.27 (d, 6H, J = 6.78 Hz, iso-C$_3$**H**$_7$–). ^{13}C NMR ($CDCl_3$, 125 MHz): δ 151.77 (s, 2C, –N–C(CH_3)=CH–**C**(CH_3)=N–), 147.07 (s, 1C, –**C**$_6$H$_4$–), 143.22 (s, 1C, –**C**$_6$H$_4$–), 143.18 (s, 2C, –N–C(CH_3)=CH–**C**(CH_3)=N–), 128.28 (d, 2C, J = 159.85 Hz, –**C**$_6$H$_4$–), 124.41 (d, 2C, J = 163.49 Hz, –**C**$_6$H$_4$–) 108.91 (d, 2C, J = 178.02 Hz, –N–C(CH_3)=**C**H–C(CH_3)=N–), 62.92 (t, 2C, J = 305.18 Hz, –N–**C**H_2–N–), 33.88 (d, 1C, J = 127.16 Hz, iso-**C**$_3$H$_7$), 25.23 (q, 2C, J = 377.84 Hz, iso-**C**$_3$H$_7$), 15.36 (q, 2C, J = 386.92 Hz, –N–C(CH_3)=CH–C(**C**H_3)=N–), 11.96 (q, 2C, J = 388.74 Hz, –N–C(**C**H_3)=CH–C(CH_3)=N–). FTIR (solid neat; cm^{-1}): ν(C–H) 2956 w; ν(C=C) 1610 s; ν(C=C) + ν(C=N)/pz ring, 1514 s, 1458 s; ν_{bend}(C–H sp^3) 1417 m; ν(N–C) 1214 s; ν_{bend}(C–H sp^2) 832 w; ν(N–M) 571 w.

2.2.5. *N*,*N*-Bis((3,5-dimethyl-1*H*-pyrazol-1-yl)methyl)-4-isopropylaniline cadmium(II) bromide [L$_B$CdBr$_2$]. A method analogous to that used to prepare **[L$_A$CoCl$_2$]** was adopted for the synthesis of **[L$_B$CdCl$_2$]**; in this case L$_B$ (0.703 g, 2.00 mmol) and $CdBr_2 \cdot 4H_2O$ (0.689 g, 2.00 mmol) to get white solid as a final product (1.16 g, 93%). Single crystals suitable for an X-ray diffraction analysis were grown by layering a CH_2Cl_2 solution of **[L$_B$CdBr$_2$]** with *n*-hexane. Analysis calculated for $C_{21}H_{29}Br_2N_5Cd$ (%): C, 40.45, H, 4.69, N, 11.24. Found: C, 40.46, H, 4.66, N, 11.20. ^{1}H NMR ($CDCl_3$, 500 MHz): δ 7.07 (d, 2H, J = 8.70 Hz, –C$_6$**H**$_4$–), 7.02 (d, 2H, J = 8.70 Hz, –C$_6$**H**$_4$–), 5.77 (s, 2H, –N–C(CH_3)=C**H**–C(CH_3)=N–), 5.88 (s, 4H, –N–C**H**$_2$–N–), 2.79–2.73 (m, 1H, J = 27.62 Hz, iso-C$_3$**H**$_7$–), 2.13 (s, 6H, N–C(CH_3)=CH–C(C**H**$_3$)=N–), 2.08 (s, 6H, –N–C(C**H**$_3$)=CH–C(CH_3)=N–), 1.14 (d, 6H, J = 6.87 Hz, iso-C$_3$**H**$_7$–). ^{13}C NMR ($CDCl_3$, 125 MHz): δ 147.56 (s, 2C, –N–C(CH_3)=CH–**C**(CH_3)=N–), 143.78 (s, 1C, –**C**$_6$H$_4$–), 141.98 (s, 1C, –**C**$_6$H$_4$–), 140.60 (s, 2C, –N–C(CH_3)=CH–**C**(CH_3)=N–), 127.55 (d, 2C, J = 156.22 Hz, –**C**$_6$H$_4$–), 119.76 (d, 2C, J = 157.13 Hz, –**C**$_6$H$_4$–) 160.97 (d, 2C, J = 174.39 Hz, –N–C(CH_3)=**C**H–C(CH_3)=N–), 64.12 (t, 2C, J = 304.27 Hz, –N–**C**H_2–N–), 33.18 (d, 1C, J = 131.70 Hz, iso-**C**$_3$H$_7$), 25.52 (q, 2C, J = 386.92 Hz, iso-**C**$_3$H$_7$), 15.00 (q, 2C, J = 365.12 Hz, –N–C(CH_3)=CH–C(**C**H_3)=N–), 11.97 (q, 2C, J = 370.57 Hz, –N–C(**C**H_3)=CH–C(CH_3)=N–). FTIR (solid neat; cm^{-1}): ν(C–H) 2960 w; ν(C=C) 1553 s; ν(C=C) + ν(C=N)/pz ring, 1510 s, 1464 s; ν_{bend}(C–H sp^3) 1418 m; ν(N–C) 1219 s; ν_{bend}(C–H sp^2) 802 w; ν(N–M) 586 w.

2.3. X-ray crystallographic studies

The X-ray-quality single crystal was coated with paratone-*N* oil, and the relevant diffraction data were collected at different levels of synchrotron radiation and at different temperatures: for the blue crystal, **[L$_A$CoCl$_2$]**, λ = 0.700 Å at 100(2) K; for the colorless crystal, **[L$_A$ZnCl$_2$]**, λ = 0.700 Å at 98(2) K; for the blue crystal, **[L$_B$CoCl$_2$]**, λ = 0.630 Å at 100(2) K; for the colorless crystal, **[L$_B$ZnCl$_2$]**, λ = 0.610 Å at 100(2) K; for the colorless crystal, **[L$_B$CdBr$_2$]**, λ = 0.700 Å at 293(2) K. These data were obtained on an ADSC Quantum-210 detector at 2D SMC with a silicon (111) double crystal monochromator (DCM) at the Pohang Accelerator Laboratory, South Korea. The PAL BL2D-SMDC program[59] was used for data collection (detector distance was 63 mm, omega scan; $\Delta\omega$ = 3°, exposure time was 1 s per frame), and HKL3000sm (Ver. 703r)[60] was used for cell refinement, reduction, and absorption correction. Structures were solved by direct methods and refined by full-matrix least-squares refinement using the SHELXL-2018 (ref. 61) computer program. The positions of all non-hydrogen atoms were refined with anisotropic displacement factors. All hydrogen atoms were placed using a riding model, and their positions were constrained relative to their parent atoms using the appropriate HFIX command in SHELXL-2014. X-ray crystallography with PLS-II 2D-SMC beamline was supported by MSIP and POSTECH.

Crystals of **[L$_B$CdBr$_2$]** were picked up with paratone-*N* oil and mounted on a Bruker SMART CCD diffractometer equipped with a graphite-monochromated Mo Kα (λ = 0.71073 Å) radiation source under a nitrogen gas cold stream (223(2) K). Data collection and integration were performed using SMART and SAINT-Plus software packages.[62] Semi-empirical absorption corrections based

on equivalent reflections were applied by SADABS.[63] The structures were solved employing direct methods and refined using a full-matrix least-squares method on F^2 using SHELXTL.[64] All non-hydrogen atoms were refined anisotropically. Hydrogen atoms were added to their geometrically ideal positions. A summary of the crystallographic refinement data is presented in Table S1.†

2.4. *rac*-Lactide polymerization

The active species for the catalysis of *rac*-LA polymerization were prepared by dissolving 0.50 mmol of the synthesized Co(II), Zn(II), and Cd(II) complexes (*i.e.*, 0.2216 g of **[L_ACoCl_2]**, 0.2248 g of **[L_A-$ZnCl_2$]**, 0.2928 g of **[L_ACdBr_2]**, 0.2407 g of **[L_BCoCl_2]**, 0.2439 g of **[L_BZnCl_2]**, and 0.3119 g of **[L_BCdBr_2]**) in 7.35 mL of THF under inert atmosphere. To these solutions was the added methyllithium (MeLi, 1.00 mmol, 0.63 mL of 1.6 M solution in Et_2O) dropwise to generate *in situ* the active catalytic species. The resulting mixture was then stirred for 2 h at room temperature, until a solution was obtained; a 1.00 mL aliquot of the said THF solution of the dimethyl Co(II), Zn(II), and Cd(II) complexes (0.0625 mmol) was then employed as initiator of the *rac*-LA ROP. **[L_nMX_2]** (L_n = L_A or L_B; M = Co or Zn, with X = Cl; M = Cd, with X = Br) itself does not exhibit any activity for ROP of *rac*-LA without MeLi, thus active species for initiation of polymerization are the combination of **[L_nMX_2]** and **MeLi** to give alkyl complex "[$LMR_{1\ or\ 2}$]" (R = Me, H, =CH_2 *etc.*). The characterization of actual catalytic species is not confirmed yet, and this pending issue will be emphasized in future work.

The general procedure for the polymerization reaction was as follows: *rac*-LA (0.901 g, 6.25 mmol) was transferred to a Schlenk flask (100 mL) under argon atmosphere, and 5.00 mL of dried CH_2Cl_2 were then added to the flask. The polymerization was initiated by the slow addition of the catalyst solution (1.0 mL, 0.0625 mmol) *via* a syringe under argon atmosphere at 25 °C and −25 °C. The reaction mixture was stirred for the specified time, and the polymerization reactions were quenched *via* addition of 1.0 mL of H_2O followed by the addition of 2.0 mL of *n*-hexane. The solvent was then evaporated directly to yield a sticky polymeric material, which was subjected to monomer conversion determination, which was monitored by integrating monomer *versus* polymer methine resonances in ^{1}H NMR spectrum. ^{1}H NMR ($CDCl_3$, 500 MHz) spectrum of the obtained polymer: δ 5.03–5.07 (m, 1H), 1.57–1.62 (m, 3H). The precipitates collected from the bulk mixture were again dissolved with CH_2Cl_2, and sequentially precipitated into *n*-hexane. Solvents were decanted, and the white solids thus isolated were first dried *in vacuo* then in a vacuum oven at 40 °C for 12 h.

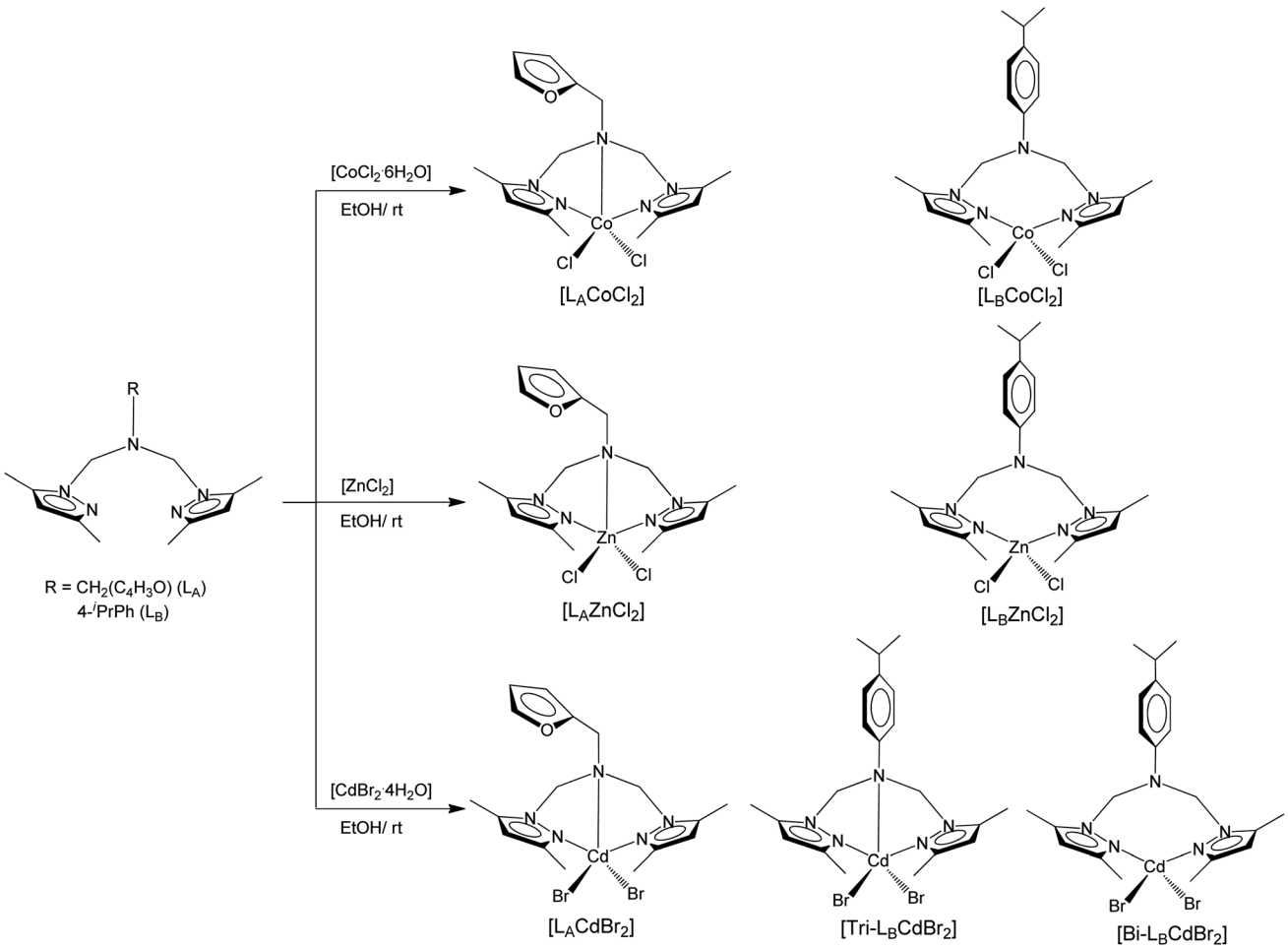

Scheme 1 Schematic representation of the synthesis of Co(II), Zn(II) and Cd(II) complexes.

Table 1 The selected bond lengths (Å) and angles (°) of $[L_nMX_2]$ ($L_n = L_A$ or L_B; M = Zn or Co, X = Cl; M = Cd, X = Br)

$[L_ACoCl_2]$		$[L_AZnCl_2]$		$[L_ACdBr_2]$	
Bond lengths (Å)					
Co(1)–N(5)	2.089(2)	Zn(1)–N(1)	2.118(4)	Cd(1)–N(5)	2.298(5)
Co(1)–N(1)	2.097(2)	Zn(1)–N(1)#1	2.118(4)	Cd(1)–N(1)	2.298(5)
Co(1)–Cl(2)	2.303(6)	Zn(1)–Cl(1)	2.264(2)	Cd(1)–Br(2)	2.562(8)
Co(1)–Cl(1)	2.327(8)	Zn(1)–Cl(2)	2.288(1)	Cd(1)–Br(1)	2.597(1)
Co(1)–N(3)	2.334(2)	Zn(1)–N(3)	2.544(5)	Cd(1)–N(3)	2.609(5)
Bond angles (°)					
N(5)–Co(1)–N(1)	110.02(6)	N(1)–Zn(1)–N(1)#1	143.4(2)	N(5)–Cd(1)–N(1)	138.5(2)
N(5)–Co(1)–Cl(2)	101.10(5)	N(1)–Zn(1)–Cl(1)	100.04(1)	N(5)–Cd(1)–Br(2)	103.51(1)
N(1)–Co(1)–Cl(2)	103.63(5)	N(1)#1–Zn(1)–Cl(1)	100.04(1)	N(1)–Cd(1)–Br(2)	105.92(2)
N(5)–Co(1)–Cl(1)	129.07(5)	N(1)–Zn(1)–Cl(2)	100.32(1)	N(5)–Cd(1)–Br(1)	99.09(1)
N(1)–Co(1)–Cl(1)	110.52(5)	N(1)#1–Zn(1)–Cl(2)	100.32(1)	N(1)–Cd(1)–Br(1)	97.18(1)
Cl(2)–Co(1)–Cl(1)	97.99(2)	Cl(1)–Zn(1)–Cl(2)	111.40(6)	Br(2)–Cd(1)–Br(1)	110.66(3)
N(5)–Co(1)–N(3)	75.04(6)	C(1)–N(1)–Zn(1)	130.6(3)	N(5)–Cd(1)–N(3)	69.87(2)
N(1)–Co(1)–N(3)	76.26(6)	N(2)–N(1)–Zn(1)	117.6(3)	N(1)–Cd(1)–N(3)	69.50(2)
Cl(2)–Co(1)–N(3)	175.70(4)	N(2)–C(6)–N(3)	107.1(4)	Br(2)–Cd(1)–N(3)	147.22(1)
Cl(1)–Co(1)–N(3)	86.01(4)	C(6)#1–N(3)–C(6)	113.5(5)	Br(1)–Cd(1)–N(3)	102.12(1)

$[L_BCoCl_2]$		$[L_BZnCl_2]$		$[Bi\text{-}L_BCdBr_2]$		$[Tri\text{-}L_BCdBr_2]$	
Bond lengths (Å)							
Co(1)–N(5)	2.034(2)	Zn(1)–N(1)	2.049(1)	Cd(1)–N(5)	2.275(5)	Cd(2)–N(10)	2.334(5)
Co(1)–N(1)	2.040(2)	Zn(1)–N(5)	2.058(1)	Cd(1)–N(1)	2.273(5)	Cd(2)–N(6)	2.381(5)
Co(1)–Cl(2)	2.235(6)	Zn(1)–Cl(1)	2.231(5)	Cd(1)–Br(1)	2.569(1)	Cd(2)–Br(3)	2.544(1)
Co(1)–Cl(1)	2.241(6)	Zn(1)–Cl(2)	2.232(5)	Cd(1)–Br(2)	2.598(1)	Cd(2)–Br(4)	2.572(1)
Co(1)–N(3)	3.864(2)	Zn(1)–N(3)	3.886(1)	Cd(1)–N(3)	2.953(4)	Cd(2)–N(8)	2.571(5)
Bond angles (°)							
N(5)–Co(1)–N(1)	110.22(6)	N(1)–Zn(1)–N(5)	109.00(5)	N(5)–Cd(1)–N(1)	120.80(2)	N(10)–Cd(2)–N(6)	137.83(2)
N(5)–Co(1)–Cl(2)	102.67(5)	N(1)–Zn(1)–Cl(1)	112.42(4)	N(5)–Cd(1)–Br(1)	112.36(1)	Br(3)–Cd(2)–Br(4)	127.20(4)
N(1)–Co(1)–Cl(2)	110.12(5)	N(5)–Zn(1)–Cl(1)	105.04(4)	N(1)–Cd(1)–Br(1)	108.16(1)	N(10)–Cd(2)–Br(3)	102.05(1)
N(5)–Co(1)–Cl(2)	112.16(4)	N(1)–Zn(1)–Cl(2)	103.19(4)	N(5)–Cd(1)–Br(2)	99.27(1)	N(6)–Cd(2)–Br(3)	99.69(1)
N(1)–Co(1)–Cl(2)	104.64(5)	N(5)–Zn(1)–Cl(2)	109.02(4)	N(1)–Cd(1)–Br(2)	108.05(1)	N(10)–Cd(2)–Br(4)	94.09(1)
Cl(2)–Co(1)–Cl(1)	117.09(2)	Cl(1)–Zn(1)–Cl(2)	118.01(2)	Br(1)–Cd(1)–Br(2)	107.02(4)	N(6)–Cd(2)–Br(4)	100.85(1)
C(1)–N(1)–Co(1)	126.88(1)	C(1)–N(1)–Zn(1)	130.22(9)	C(1)–N(1)–Cd(1)	136.1(4)	N(10)–Cd(2)–N(8)	69.83(2)
N(2)–N(1)–Co(1)	126.81(1)	N(2)–N(1)–Zn(1)	123.23(8)	N(2)–N(1)–Cd(1)	118.9(3)	N(6)–Cd(2)–N(8)	68.79(2)
N(3)–C(6)–N(2)	111.16(1)	N(3)–C(6)–N(2)	113.53(1)	N(2)–C(6)–N(3)	108.3(4)	Br(3)–Cd(2)–N(8)	132.44(1)
N(3)–C(7)–N(4)	113.55(1)	N(3)–C(7)–N(4)	111.23(1)	N(3)–C(7)–N(4)	108.3(4)	Br(4)–Cd(2)–N(8)	100.34(1)

Note: Proper precautionary measures need to be taken for handling alkyl-cadmium species, prepared for ROP reaction, owing to their pulmonary toxicity.

3. Results and discussion

3.1. Synthesis and physical parameters

In the current investigation *N*,*N*-bis((3,5-dimethyl-1*H*-pyrazol-1-yl)methyl derivatives were selected to study the effects of the ligand substitution patterns on the polymerization behavior. For instance, the amine moiety possessing an identical *N*,*N*-bis((3,5-dimethyl-1*H*-pyrazol-1-yl)methyl framework was modified/varied from to furanyl-methanamine (L_A) and isopropylaniline (L_B) to investigate how the steric effects and electronic properties affect the catalytic performance and stereoselectivity of the *N*,*N*-bis((3,5-dimethyl-1*H*-pyrazol-1-yl) methyl-based Zn(II), Co(II), and Cd(II) complexes toward the ROP of *rac*-LA. The ligands were prepared *via* a single-step condensation reaction involving furfurylamine or/and 4-isopropylaniline and 3,5-dimethyl-1*H*-pyrazolyl-1-methanol, as outlined in Scheme S1.† The reaction of ligands L_A and L_B with $CoCl_2 \cdot 6H_2O$, $ZnCl_2$, and $CdBr_2 \cdot 4H_2O$ in 1 : 1 molar ratio led to the formation of the desired complexes of $[L_nMX_2]$ ($L_n = L_A$ or L_B; M = Co or Zn, with X = Cl; M = Cd, with X = Br) general formula in good yield (Scheme 1).

The FTIR spectra of the synthesized complexes were characterized by the presence of absorption bands corresponding to the ν(C=N) and ν(C=C) stretching frequencies of the pyrazolyl motif in the 1514–1493 cm^{-1} and 1464–1458 cm^{-1} wavenumber ranges, respectively. These values compare favorably to the corresponding ones reported for other complexes in the literature.[65] In the spectra of the complexes, the absorption bands due to the stretching of aromatic C=C and C–H bonds were observed to shift to higher wavenumbers with respect to the corresponding free ligands. Similarly, the complexes' absorption bands due to the stretching of sp^3 and sp^2 C–H and C=C

bonds appeared at the expected wavenumbers, based on literature data.[50,51,66] Additionally, the C–O bond stretching appeared in the 1110–1230 cm^{-1} wavenumber range, in the case of **[L_BMX_2]** (M = Zn(II) or Co(II), with X = Cl; M = Cd(II), with X = Br). The absorption bands assigned to the stretching of the $(C{=}N)_{pyrazole}$ bond shifted to higher wavenumbers in the FTIR spectra of **[L_nMX_2]** complexes with respect to the corresponding (free) ligands, which suggests the possibility of a back-donation and the involvement of the nitrogen atoms of pyrazolyl or/and amine moieties in metal bonding.[67] The newly confirmed bands appearing in the 599–570 cm^{-1} wavenumber range were attributed to the ν(M–N) stretching frequencies (M = Zn(II), Co(II), or Cd(II)).[68]

Compositional analysis data of the synthesized complexes are consistent with the proposed formulas reported in Scheme 1 and confirmed the purity of the isolated complexes. ^{1}H NMR and ^{13}C NMR spectroscopy data on the Zn(II) and Cd(II) complexes revealed the formation of the expected chemical species and were consistent with the synthesis of mononuclear structures.

3.2. Solid state structures of Co(II), Zn(II) and Cd(II) complexes

The solid-state structures of the synthesized Co(II), Zn(II), and Cd(II) complexes were elucidated by single-crystal X-ray diffraction studies. The geometric parameters defining the coordination environment of the complexes are listed in Table 1; in Fig. 1–6, on the other hand, are reported the ORTEP diagrams of **[L_ACoCl_2]**, **[L_AZnCl_2]**, **[L_ACdBr_2]**, **[L_BCoCl_2]**, **[L_BZnCl_2]**, and **[L_BCdBr_2]**, respectively. The M(II) center in **[L_AMX_2]** (M = Co, Zn, or Cd; X = Cl or Br) was observed to be coordinated in tridentate fashion by the nitrogen atoms of the pyrazolyl and amine moieties of the bis(pyrazolylamine) ligand, thus forming two five-membered chelate rings (Fig. 1–3).[51,66,69]

[L_ACoCl_2] and **[L_AZnCl_2]** exhibited distorted trigonal bipyramidal geometries, whereas the geometry of **[L_ACdBr_2]** can be best described as distorted square pyramidal. The M–$N_{pyrazole}$ bond lengths are 2.089(2) and 2.097(2) Å for **[L_ACoCl_2]**, 2.118(4) and 2.118(4) Å for **[L_AZnCl_2]**, 2.298(5) and 2.298(5) Å for **[L_ACdBr_2]**. The M–N_{amine} bond distances for these complexes have values within the expected range (2.334(2)–2.609(5) Å).[50,66,70] The X-ray diffraction data revealed that the Co–$N_{pyrazole}$ bonds are slightly shorter than the Co–N_{amine} bonds, probably because of the basicity difference between amine and pyrazole nitrogens. The M–Cl and M–Br bond distances had values in the 2.327(8)–2.264(2) Å and 2.597(1)–2.562(8) Å ranges, respectively. $N_{pyrazole}$–M–$N_{pyrazole}$ bond angles were found to have values of 110.02(6)° **[L_ACoCl_2]**, 143.4(2)° **[L_AZnCl_2]**, and 138.5(2)° **[L_ACdBr_2]**. The $Cl_{terminal}$–M–$Cl_{terminal}$ bond angle had values of 97.99(2)° and 111.40(6)° for **[L_ACoCl_2]**, and 143.4(2)° for **[L_AZnCl_2]**, respectively,; the $Br_{terminal}$–M–$Br_{terminal}$ bond angle of **[L_ACdBr_2]** was observed to measure 110.66(3)°. X-ray data also revealed that the $N_{pyrazole}$–M–$N_{pyrazole}$ bond angles had much smaller values than the $Cl_{terminal}$–M–$Cl_{terminal}$ or $Br_{terminal}$–M–$Br_{terminal}$ bite angles

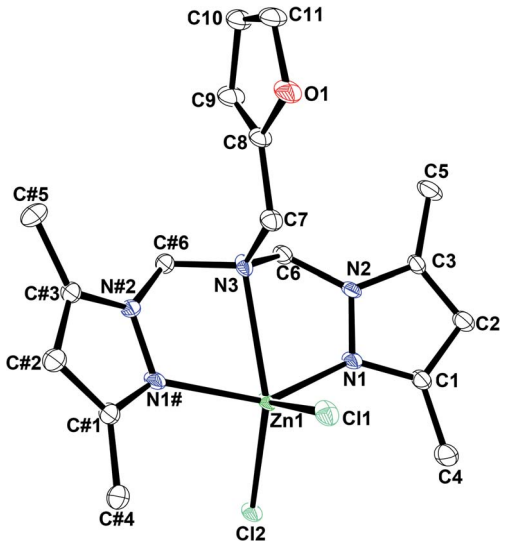

Fig. 2 An ORTEP drawing of [L_AZnCl_2] with thermal ellipsoids at 50% probability. All hydrogen atoms are omitted for clarity.

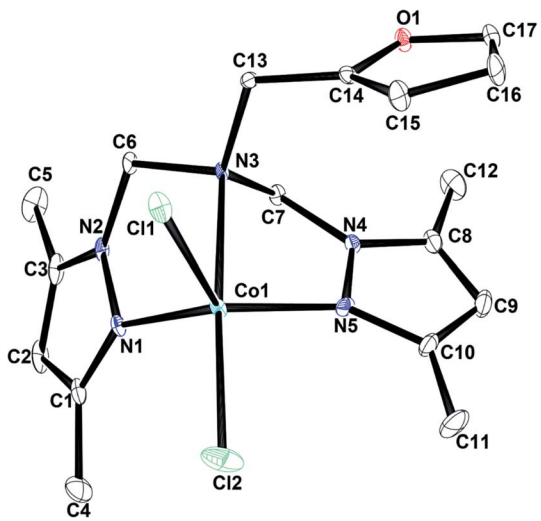

Fig. 1 An ORTEP drawing of [L_ACoCl_2] with thermal ellipsoids at 50% probability. All hydrogen atoms are omitted for clarity.

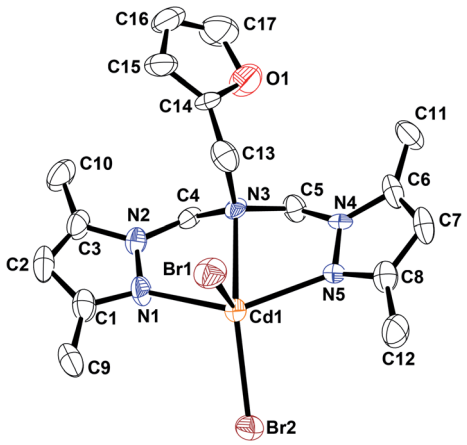

Fig. 3 An ORTEP drawing of [L_ACdBr_2] with thermal ellipsoids at 50% probability. All hydrogen atoms are omitted for clarity.

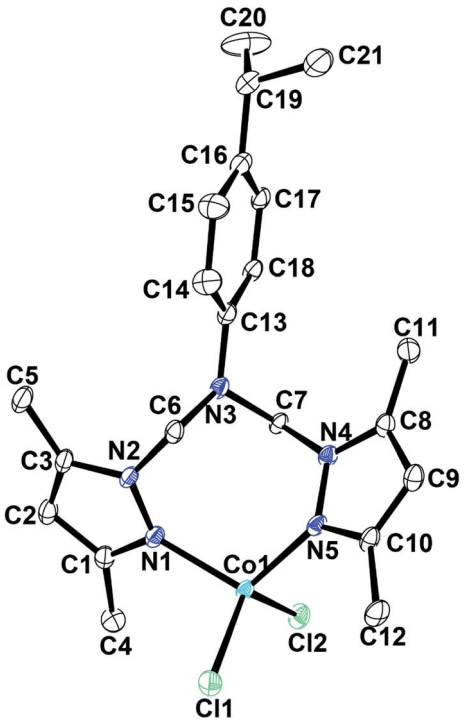

Fig. 4 An ORTEP drawing of $[L_BCoCl_2]$ with thermal ellipsoids at 50% probability. All hydrogen atoms are omitted for clarity.

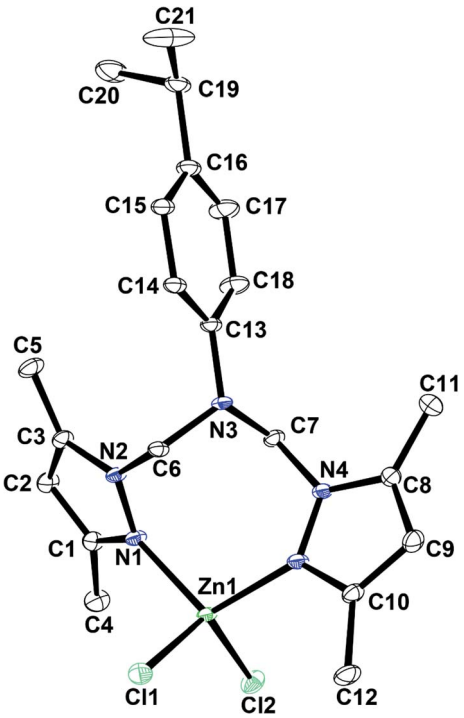

Fig. 5 An ORTEP drawing of $[L_BZnCl_2]$ with thermal ellipsoids at 50% probability. All hydrogen atoms are omitted for clarity.

(Table 1), a common attribute of $[LMX_2]$-type complexes with tetrahedral geometry.

Interestingly, the potentially tridentate ligand L_B did not engage in the expected tridentate coordination of the M(II) centers but displayed a bidentate coordination mode, whereby ligation occurred *via* the nitrogen atoms of pyrazolyl moieties. **$[L_BCoCl_2]$** and **$[L_BZnCl_2]$** exhibited distorted tetrahedral geometries around the metal centers, as a result of the metal ions being coordinated by the *N*-substituted bis(pyrazolylamine) ligand in bidentate fashion and by two halide ions (Fig. 4 and 5).[68] The $M–N_{pyrazole}$ bond distances in **$[L_BCoCl_2]$** and **$[L_BZnCl_2]$** have values of 2.037 and 2.054 Å, respectively; notably, these geometric parameters are in good agreement with the accepted values.[66] Similarly, the M–Cl and M–Br bond distances of these complexes are comparable to the bond lengths reported for structurally related Zn(II) compounds.[66] Furthermore, the $N_{pyrazole}–M–N_{pyrazole}$ bond angles had values of 110.22(6)° for **$[L_BCoCl_2]$** and 109.00(5)° for **$[L_BZnCl_2]$**, whereas the values for the $Cl_{terminal}–M–Cl_{terminal}$ bond angles lie in the 102.67(5)°–112.42(4)° range.

Contrarily, the ORTEP diagram of **$[L_BCdBr_2]$** illustrates that this complex has two crystal structures in one unit cell. These crystal structures are depicted in Fig. 6 and S59,† with values for relevant selected parameters listed in Table 1.

In the crystalline phase, this complex has two crystallographically independent Cd(II) sites: one Cd is tetra-coordinated and displays a tetrahedral structure whereas the other is penta-coordinated and displays a square pyramidal geometry. Addison *et al.*[71] have introduced index of trigonality, τ, which provides useful information regarding the geometry of five-coordinate complexes; in particular, a perfect trigonal bipyramidal geometry is characterized by value of τ_5 of 1.0 whereas a value for τ_5 of 0.0 is indicative of a perfect square pyramidal geometry. Where $\tau = (\beta - \alpha)/60$, in which α and β are the two largest coordination angles as illustrated in τ_5 values (Table S2†).[71–74] In the case of the five-coordinate Cd center in **$[L_BCdBr_2]$** in the crystalline phase, t was found to have a value of 0.089; hence this Cd center was concluded to exhibit a distorted square pyramid five-coordinate geometry. Notably, in the mentioned structure, the amine nitrogen occupies the apex of the square pyramid. All the bond lengths and angles around the Cd center in both structures are in agreement with those reported previously for tetra- and/or penta-coordinated Cd(II) complexes.[69,75] Additionally, the geometry of **$[L_ACdBr_2]$** (τ_5 = 0.145) could be described as distorted square pyramidal whereas the geometries of **$[L_ACoCl_2]$** ($\tau_5 = 0.777$) and **$[L_AZnCl_2]$**, (τ_5 = 0.533) could be described as distorted trigonal bipyramidal (Table S2†). The angles between the $X_1–M–X_2$ (X = Cl or Br) and $N_{pyrazole}–M–N_{pyrazole}$ planes in **$[L_ACoCl_2]$**, **$[L_AZnCl_2]$**, **$[L_ACdBr_2]$**, and **$[L_BCdBr_2]$** were observed to have values of 95.83(4)°, 90.00(2)°, 91.34(1)°, and 87.12(1)°, respectively.

The geometry of tetra-coordinated complexes can be described by the value of the τ_4 parameter. Specifically, in the case of a perfect tetrahedron, τ_4 has a value of 1.00 whereas its value is equal to 0.00 in the case of a perfect square planar geometry.[76] The values of the τ_4 parameters for the tetra-coordinated complexes **$[L_BCoCl_2]$**, **$[L_BZnCl_2]$**, and **$[L_BCdBr_2]$** are listed in Table S3.†[76] Based on these values, the geometry around the M(II) centers of the these complexes could be concluded to be distorted tetrahedral. Additionally, the bond angles around the Co(II), Zn(II), and Cd(II) centers were

employed to measure the degree of distortion. The calculated angles between the X_1–M–X_2 (X = Cl or Br) and $N_{pyrazole}$–M–$N_{pyrazole}$ planes of **[L_BCoCl$_2$]**, **[L_BZnCl$_2$]**, and **[L_BCdBr$_2$]** were 95.11(4)°, 94.49(3)°, and 94.69(9)°, respectively.

3.3. *rac*-Lactide polymerization

The catalytic capabilities of 3,5-dimethylpyrazolylamine based Co(II), Zn(II), and Cd(II) initiators, were tested for *rac*-LA polymerization at two different temperatures. The catalytic species were generated *in situ* by treating dichloro Co(II), Zn(II) and dibromo Cd(II) complexes with two equiv. of MeLi in THF. The alkyl derivatives proved significantly active, allowing conversion of *rac*-LA at 25 °C and −25 °C, inspected by the decrease of monomer signals in ^{1}H NMR spectrum of the resultant PLA. Representative polymerization results are summarized in Tables 2 and 3. The complete conversion was observed within 2 h, where 98% conversion was achieved for L_B-containing Zn complex after 5 min of reaction at 25 °C, as revealed by the %-conversion *vs.* time plot (Fig. S60†).

The experimentally determined M_n (corrected using the Mar–Houwink factor of 0.58)[77] had values that were half of those calculated based on the monomer/initiator molar ratio. This observation could be explained by assuming the presence of two growing polymer chains per metal center. Notably, the molecular weights of the resultant PLAs were also influenced by the identity of the M(II) center. In fact, as Cd(II) was replaced by Co(II), the M_n value of the produced PLAs appeared to decrease (Table 2). A general trend was observed toward a linear increase in the M_n value as the polymerization time increased (Fig. S61†). For example, the value of M_n was 6.28 × 10^3 g mol^{-1} for 1 min, 8.20 × 10^3 g mol^{-1} for 3 min, 8.81 × 10^3 g mol^{-1} for 5 min, and 9.64 × 10^3 g mol^{-1} for 10 min polymerization time (Fig. S62–S65†). However, the conversion rate did not increase after 5 min; in the case of the L_B containing Zn-complex. The plot of the M_n values *versus* the monomer/catalyst ratio indicated that an increase in monomer/catalyst ratio was associated with a linear increase in the M_n values observed up to *rac*-LA/catalyst = 400 (Fig. S66†). For example, with an increase in the *rac*-LA/catalyst ratio from 100 to 400, increase in the M_n values from 9.27 × 10^3 g mol^{-1} to 19.26 × 10^3 g mol^{-1}, respectively, is observed. However, with an increase in the monomer/catalyst ratio from 400 to 500 a decrease in M_n values have been observed (Fig. S67–S71†). Additionally, the % conversion value was not substantially affected by increases in the monomer/catalyst ratio. The M_n of the resultant PLAs was in turn slightly affected by the identity of the amine substituents. For instance, the M_n values of the PLAs obtained *via* catalysis with the L_A-containing complexes were higher than their counterparts measured for the PLAs synthesized using the L_B-containing complexes as catalysts, as illustrated by the polymerization data collected (Table 3; entries 2, 4, and 6). This trend contradicted those reported recently for catalysts consisting of Zn(II) and Cu(II) complexes bearing (pyrazol-1-ylmethyl)pyridine ligands, whereby increases in the steric bulk of the amine substituents attached to the ligand framework were associated with increases in the molecular weight of the polymers produced.[39] However, in the cases of the hereby studied initiators, the observed M_n values were lower compared to the calculated ones (Tables 2 and 3), probably because of the low initiation efficiencies of these complexes which resulted in a broader range of PDIs (1.36–2.23).[78] However, the PDIs values notably decrease (1.16–1.52) as the polymerization temperature decreases from 25 °C to −25 °C (Table 3).

Generally, the steric hindrance around the M(II) center caused by increases in the bulk of ligand substituents/groups

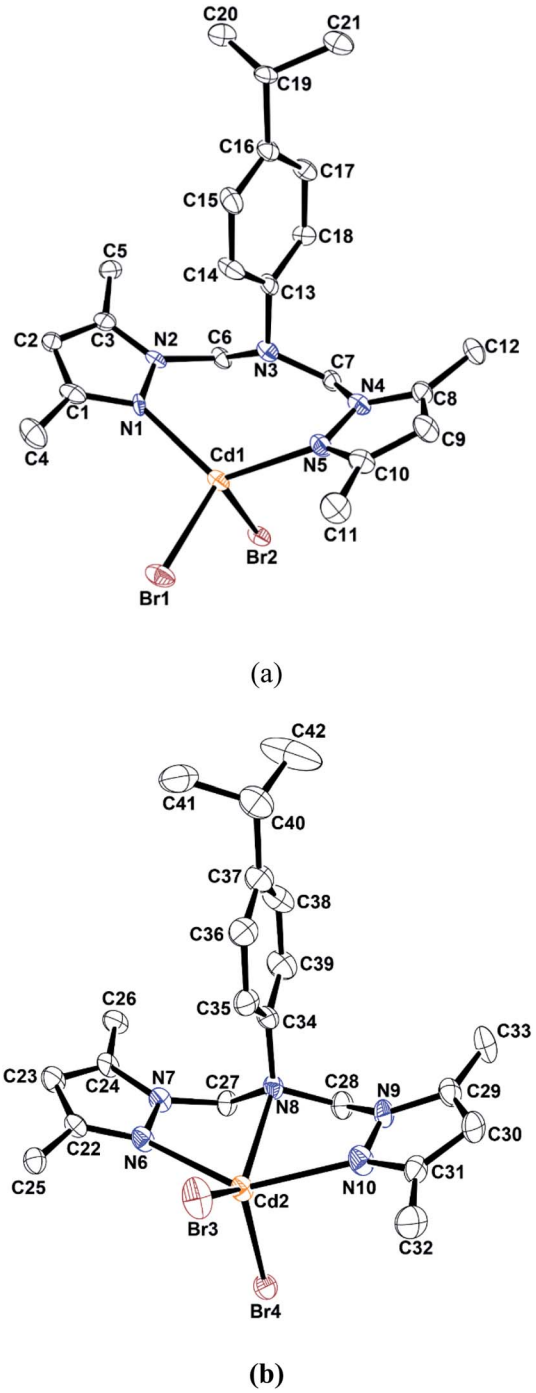

Fig. 6 An ORTEP drawing of tetrahedral [Bi-L_BCdBr$_2$] (a) and square pyramidal [Tri-L_BCdBr$_2$] (b) with thermal ellipsoids at 50% probability. All hydrogen atoms are omitted for clarity.

Table 2 Polymerization of *rac*-LA with catalytic species generated *in situ* from the reaction of **[L_nMX_2]** ($L_n = L_A$ and L_B, M = Co, Zn, X = Cl; M = Cd, X = Br) and MeLi in CH_2Cl_2 at 25 °C

Entry	Catalyst[a]	Conv.[b] (%)	M_n[c] (g mol^{-1}) × 10^3 (calcd.)	M_n[d] (g mol^{-1}) × 10^3 (GPC)	M_w[d] (g mol^{-1}) × 10^3 (GPC)	PDI[d]	P_r[e]
1	**MeLi**	99	14.27	11.44	17.21	1.50	0.47
2	**[L_ACoCl_2]/MeLi**	98	14.12	8.57	15.57	1.82	0.53
3	**[L_BCoCl_2]/MeLi**	98	14.12	11.34	15.43	1.36	0.82
4	**[L_AZnCl_2]/MeLi**	98	14.12	8.18	18.28	2.23	0.53
5	**[L_BZnCl_2]/MeLi**	97	13.98	8.02	12.16	2.02	0.68
6	**[L_ACdBr_2]/MeLi**	98	14.12	8.04	12.72	2.11	0.51
7	**[L_BCdBr_2]/MeLi**	98	14.12	5.39	10.19	1.89	0.60

[a] Conditions: [initiator] = 0.0625 mmol, [*rac*-LA]/[initiator] = 100; 5.0 mL of CH_2Cl_2 as polymerization solvent; polymerization time = 2 h. [b] Monomer conversion (%) determined by ^{1}H NMR spectroscopy. [c] Calculated from ([molecular weight of *rac*-LA] × [mol concentration of used [*rac*-LA]/[mol concentration of initiator]) × (conversion%). [d] Determined by gel permeation chromatography (GPC) in THF, relative to polystyrene standard (corrected using the Mark–Houwink factor of 0.58).[77] [e] Probability of heterotactic enchainment (P_r) were calculated on the basis of homonuclear decoupled ^{1}H NMR spectra according to literature.[55–58]

reduce the catalytic activity of the complex.[79–81] In fact, changing the amine moiety from furanyl-methanamine to isopropylaniline did not significantly affect the catalytic activity of the hereby investigated complexes. This fact is further augmented by the calculation of buried volumes using SambVca program.[82] The total steric hindrance provided by ligand with respect to the metal center can be quantitatively calculated by comparing the topographic steric maps of the various M(II) complexes (M = Co, Zn, and Cd). Ball and stick models, space-filling models, and topographic steric maps of these complexes are presented in Fig. S72.† Evidence indicates that, for a particular metal center, five-coordinated complexes are characterized by larger buried volumes than four-coordinated complexes, although these differences did not translate into significant differences in catalytic activity.

A monomer-activated mechanism can be predicted to take place in the case of the ROP of *rac*-LA initiated by the types of dimethyl-containing M(II) species investigated in the present study.[83] In this mechanistic approach, the monomer would be electronically activated as a result of its coordination to the electrophilic M(II) center. Simultaneously, one of the metal-bound methyl groups nucleophilically attacks the carbonyl carbon of the monomer to initiate the ROP of the lactide by breaking the bond between the endocyclic oxygen and the carbonyl group. This step contrasts with the classical coordination insertion mechanism,[84] whereby the opening of the ring occurs *via* the nucleophilic reactivity of a δ-bonded alkyl/alkoxide group that is bound to the M(II) center. Furthermore, the propagation proceeded by the attack, which contributed to the growth of the polymer chain at the M end, after which the addition of the LA molecule produced the heterotactic PLA. The ROP-initiating solution was predicted to comprise some unreacted MeLi along with the *in situ*-generated dimethyl M(II) (M = Co, Zn, and Cd) species. Notably, the polymerization reaction conducted in the presence of MeLi only (Table 2; entry 1) furnished PLA with good conversion (99% in 2 h) but with negligible stereoselectivity (P_r = 0.47 at 25 °C). Additionally, the activity using MeLi alone is low as illustrated in Fig. S73;† a negligible amount of PLA has been obtained after 5 min of reaction time comparted to **[L_BZnCl_2]/MeLi** system which give 98% conversion within 5 min of reaction time (Fig. S60†). These results highlighted the benefits afforded by the Lewis acidic M(II) center and the bis(pyrazolyl-amine) framework; indeed, use of the resulting complex as catalyst delivered good polymerization control and directed the heterotacticity of the resultant PLA. Moreover, conducting the ROP reaction using **[L_nMX_2]** ($L_n = L_A$ or L_B; M = Co or Zn, with X = Cl; M = Cd, with X = Br) in the absence of MeLi resulted in negligible amounts of PLA.[31,85]

Table 3 Polymerization of *rac*-LA with catalytic species generated *in situ* from the reaction of **[$LnMX_2$]** ($L_n = L_A$ and L_B, M = Co, Zn, X = Cl; M = Cd, X = Br) and MeLi in CH_2Cl_2 at −25 °C

Entry	Catalyst[a]	Conv.[b] (%)	M_n[c] (g mol^{-1}) × 10^3 (calcd.)	M_n[d] (g mol^{-1}) × 10^3 (GPC)	M_w[d] (g mol^{-1}) × 10^3 (GPC)	PDI[d]	P_r[e]
1	**MeLi**	99	14.27	9.945	16.49	1.66	0.78
2	**[L_ACoCl_2]/MeLi**	97	13.98	7.77	11.80	1.52	0.69
3	**[L_BCoCl_2]/MeLi**	97	13.98	6.42	8.64	1.35	0.82
4	**[L_AZnCl_2]/MeLi**	97	13.98	6.57	8.20	1.25	0.85
5	**[L_BZnCl_2]/MeLi**	97	13.98	6.52	7.56	1.16	0.94
6	**[L_ACdBr_2]/MeLi**	97	13.98	10.12	14.03	1.39	0.80
7	**[L_BCdBr_2]/MeLi**	98	14.12	4.71	7.06	1.50	0.69

[a] Conditions: [initiator] = 0.0625 mmol, [*rac*-LA]/[initiator] = 100; 5.0 mL of CH_2Cl_2 as polymerization solvent; polymerization time = 2 h. [b] Monomer conversion (%) determined by ^{1}H NMR spectroscopy. [c] Calculated from ([molecular weight of *rac*-LA] × [mol concentration of used *rac*-LA]/[mol concentration of initiator]) × (conversion%). [d] Determined by gel permeation chromatography (GPC) in THF, relative to polystyrene standard (corrected using the Mark–Houwink factor of 0.58).[77] [e] Probability of heterotactic enchainment (P_r) were calculated on the basis of homonuclear decoupled ^{1}H NMR spectra according to literature.[55–58]

The stability of the studied systems was determined implementing a sequential five-stage *rac*-LA polymerization reaction using **[L_BZnCl_2]/MeLi** system at 25 °C (Table S4; Fig. S60†). In the first cycle, 98% conversion was achieved within 5 min, in conditions whereby [*rac*-LA]/[initiator] = 100. Subsequently, another 100 equivalents of monomer were added to the reaction mixture ([*rac*-LA]/[initiator] = 200), and a conversion value of 93% was measured without the addition of initiator. A slight drop in the activity signifies the stability of the said initiator. Afterwards, sequential additions of 100 equivalents of the monomer were performed at interval of 5 min, and at [*rac*-LA]/[initiator] = 500, the conversion was observed to have a value of 67%.

The PLAs produced using **[L_nMCl_2]/MeLi** (L_n = L_A or L_B, M = Co or Zn, with X = Cl; M = Cd, with X = Br) as catalysts are predominantly heterotactic. Polymerization results indicated that the preference for heterotactic bias was relatively low when the reaction temperature was 25 °C (P_r = 0.51–0.82 at 25 °C, Table 2), which is consistent with our previously published findings.[86,87] However, a drop in reaction temperature from 25 to −25 °C resulted in increased heteroselectivity (P_r = 0.68–0.94). Polymerization data further revealed that the L_B-containing complexes bearing the isopropylaniline moiety (*i.e.*, **[L_BMCl_2]/MeLi**) afforded superior heteroselectivities at 25 °C to their L_A-containing counterparts (Table 2). Thus, enhancing the bulk of the amine moiety was observed to result in an increase of the heterotacticity of the PLAs produced using the studied complexes as catalysts. However, when polymerization was conducted at −25 °C, the opposite trend became apparent (Table 3). The proper orientation of the substituents in the ancillary ligand could thus provide the electronic environment for the effective accommodation of any possible steric clash between the ligand and the propagating PLA chain and the alternative attachment of the incoming monomer molecule. These results indicate that the polymerization of *rac*-LA monomers catalyzed by the hereby developed catalytic system proceeded by the chain end mechanism. These findings are in good agreement with the results of our previously published studies.[50,86,87]

The catalytic activity of the Zn(II) system in the context of *rac*-LA polymerization are comparable with those reported by our group for dimethyl Zn(II) complexes, but use of the hereby developed system yielded PLAs with higher heterotacticity than we reported at 25 °C.[87] In comparison with the previously reported Zn(II) system bearing *N*,*N*′,*N*-bis((1*H*-pyrazol-1-yl)methyl)amines derivatives as ligands (P_r = 0.95 at −50 °C with 90% conversion), the current system exhibited higher activity and comparable heteroselectivity (97% conversion with P_r = 0.94 at −25 °C).[49] Moreover, in comparison with the complexes of the tetradentate *N*,*N*,*N*,*N*-bis(pyrazolyl)methane ligand with Zn(II) and Fe(II) (P_r = 0.79) used as catalysts,[88] our system exhibited superior activity and stereoselectivity (P_r = 0.94). Co(II)-based catalysts previously studied by our group, comprising *N*,*N*-bis((3,5-dimethyl-1*H*-pyrazol-1-yl)methyl)-3,5-dimethylaniline and *N*,*N*-bis((3,5-dimethyl-1*H*-pyrazol-1-yl)methyl)-4-methoxyaniline as ligands, afforded PLAs of lower molecular weight and heterotacticity (P_r = 0.81–0.85 at −50 °C) but narrower PDI value range (1.13–1.21).[50] Recently, Sutar *et al.* described the ROP of L-lactide catalyzed by the Co(II)–salen complex, which afforded 79% conversion at 30 °C after 24 h with a narrow range of MWD values (1.12).[89] In comparison with the hereby developed Co(II)-based catalytic system, the recently reported co-tripodal complexes/^{i}PrOH catalytic system proved to be effective, affording 81% conversion within 2 min to produce isotactic PLA (P_m = 0.73).[90] Chakraborty's group demonstrated that $CoCl_2 \cdot 6H_2O$ could effectively catalyze the polymerization of *rac*-LA, affording 96% conversion within 1 h under melting conditions (145 °C), albeit with negligible stereocontrol.[91] Mandal *et al.* recently reported that $Cd(OAc)_2$ was an effective catalyst in the presence of benzyl alcohol at 140 °C; in fact, use of this catalyst afforded 98% conversion within 18 min (monomer-: [Cd] : BnOH ratio = 100 : 1 : 2).[92] Similarly, the Cd(II) complexes from this recent investigation achieved the complete conversion of the monomer to PLA with stereoselectivities that were equivalent to those achieved using Cd(II) complexes with the *N*,*N*′,X-tridentate iminomethylpyridine ligand framework.[93] Further research work should focus on the design and optimization of procedures that afford the production of PLAs with improved polymerization control and enhanced stereoregularity.

4. Conclusions

We demonstrated the synthesis of Co(II), Zn(II), and Cd(II) complexes supported with *N*,*N*-bis((3,5-dimethyl-1*H*-pyrazol-1-yl)methyl)amines derivatives and determined their crystal structures by X-ray diffraction. Diverse coordination geometries were afforded through the bi- and/or tri-dentate coordination of the ligands to the M(II) centers *via* the nitrogen atoms of the ligands' pyrazole and amine moieties. **[L_nMX_2]/MeLi** (L_n = L_A or L_B, M = Co or Zn, with X = Cl; M = Cd, with X = Br) system effectively catalyzed the ROP of *rac*-LA to yield low-molecular-weight PLAs with a broader range of PDI values (1.36–2.11). The catalytic performance of the initiators was observed to depend to a minor extent on the ligand substitution pattern. Based on the polymerization results, the introduction of substituents that increased steric hindrance around the M(II) center increased the amount of heterotactic enchainment along the growing polymer chain.

Author contributions

Solhye Choe: formal analysis-supporting. Hyosun Lee: conceptualization; supervision-lead. Saira Nayab: writing original draft-supporting.

Conflicts of interest

There are no conflicts to declare.

Acknowledgements

This research was supported by the National Research Foundation (NRF) of South Korea, funded by the Ministry of the Education, Science, and Technology (MEST) (Grant No. 2019R1A2C1088654). This work was also supported by the Technology Innovation Program (TIP # 20011123, Development

of Cyclic Olefin Polymer(COP) with High Heat Resistance and High Transmittance) funded by the Korea Evaluation Institute of Industrial Technology (KEIT) and the Ministry of Trade, Industry & Energy (MOTIE, Republic of Korea). This work has also been supported by Higher Education Commission (HEC), Islamabad, Islamic Republic of Pakistan, under National Research Programme for Universities (NRPU) Grant No. 6840-KP. X-ray crystallography with PLS-II 2D-SMC beamline was supported by MSIP and POSTECH.

References

1 R. E. Drumright, P. R. Gruber and D. E. Henton, *Adv. Mater.*, 2000, **12**, 1841–1846.
2 A. Amgoune, C. M. Thomas, T. Roisnel and J.-F. Carpentier, *Chem.–Eur. J.*, 2006, **12**, 169–179.
3 R. P. Brannigan and A. P. Dove, *Biomater. Sci.*, 2017, **5**, 9–21.
4 M. A. Ghalia and Y. Dahman, *J. Polym. Res.*, 2017, **74**, 24–45.
5 E. Chiellini and R. Solaro, *Adv. Mater.*, 1996, **8**, 305–313.
6 A.-C. Albertsson and I. K. Varma, *Biomacromolecules*, 2003, **4**, 1466–1486.
7 H. Sun, J. S. Ritch and P. G. Hayes, *Inorg. Chem.*, 2011, **50**, 8063–8072.
8 R. Petrus and P. Sobota, *Organometallics*, 2012, **31**, 4755–4762.
9 B. Gao, X. Li, R. Duan, Q. Duan, Y. Li, X. Pang, H. Zhuang and X. Chen, *RSC Adv.*, 2015, **5**, 29412–29419.
10 S. Ghosh, R. R. Gowda, R. Jagan and D. Chakraborty, *Dalton Trans.*, 2015, **44**, 10410–10422.
11 G. Li, M. Lamberti, D. Pappalardo and C. Pellecchia, *Macromolecules*, 2012, **45**, 8614–8620.
12 C. Bakewell, R. H. Platel, S. K. Cary, S. M. Hubbard, J. M. Roaf, A. C. Levine, A. J. P. White, N. J. Long, M. Haaf and C. K. Williams, *Organometallics*, 2012, **31**, 4729–4736.
13 W. Yang, K.-Q. Zhao, T. J. Prior, D. L. Hughes, A. Arbaoui, M. R. J. Elsegood and C. Redshaw, *Dalton Trans.*, 2016, **45**, 11990–12005.
14 W. Zhang, Y. Wang, L. Wang, C. Redshaw and W.-H. Sun, *J. Organomet. Chem.*, 2014, **750**, 65–73.
15 S. Tabthong, T. Nanok, P. Sumrit, P. Kongsaeree, S. Prabpai, P. Chuawong and P. Hormnirun, *Macromolecules*, 2015, **48**, 6846–6861.
16 A. Thevenon, C. Romain, M. S. Bennington, A. J. P White, H. J. Davidson, S. Brooker and C. K. Williams, *Angew. Chem., Int. Ed.*, 2016, **55**, 8680–8685.
17 T. Rosen, Y. Popowski, I. Goldberg and M. Kol, *Chem.–Eur. J.*, 2016, **22**, 11533–11536.
18 D. Jedrzkiewicz, G. Adamus, M. Kwiecień, Ł. John and J. Ejfler, *Inorg. Chem.*, 2017, **56**, 1349–1365.
19 A. B. Kremer, R. J. Andrews, M. J. Milner, X. R. Zhang, T. Ebrahimi, B. O. Patrick, P. L. Diaconescu and P. Mehrkhodavandi, *Inorg. Chem.*, 2017, **56**, 1375–1385.
20 T. Rosen, I. Goldberg, V. Venditto and M. Kol, *J. Am. Chem. Soc.*, 2016, **138**, 12041–12044.
21 C. -Y. Li, S. -J. Hsu, C. -I. Lin, C. -Y. Tsai, J. -H. Wang, B. -T. Ko, C. -H. Lin and H. -Y. Huang, *J. Polym. Sci., Part A: Polym. Chem.*, 2013, **51**, 3840–3849.
22 S. Fortun, P. Daneshmand and F. Schaper, *Angew. Chem., Int. Ed.*, 2015, **54**, 13669–13672.
23 J. Zhang, B. Wang, L. Wang, J. Sun, Y. Zhang, Z. Cao and Z. Wu, *Appl. Organomet. Chem.*, 2017, 4077–4085.
24 D. M. Lyubov, A. O. Tolpygin and A. A. Trifonov, *Coord. Chem. Rev.*, 2019, **392**, 83–145.
25 M. Hu, F. Han, W. Zhang, W. Ma, Q. Deng, W. Song, H. Yan and G. Dong, *Catal. Sci. Technol.*, 2017, **7**, 1394–1403.
26 M. J. Stanford and A. P. Dove, *Chem. Soc. Rev.*, 2010, **39**, 486–494.
27 R. H. Platel, L. M. Hodgson and C. K. Williams, *Polym. Rev.*, 2008, **48**, 11–63.
28 W. A. Munzeiwa, V. O. Nyamori and B. Omondi, *Appl. Organomet. Chem.*, 2018, **32**, 4247–4256.
29 T. J. J. Whitehorne and F. Schaper, *Inorg. Chem.*, 2013, **52**, 13612–13622.
30 J. Cho, M. K. Chun, S. Nayab and J. H. Jeong, *Transition Met. Chem.*, 2019, **44**, 175–185.
31 K. S. Kwon, S. Nayab and J. H. Jeong, *Polyhedron*, 2017, **130**, 23–29.
32 K. D. Pressing, J. H. Lehr, M. E. Pratt, L. N. Dawe, A. A. Sarjeant and C. M. Kozak, *Dalton Trans.*, 2015, **44**, 12365–12375.
33 L. Chen, W. Li, D. Yuan, Y. Zhang, Q. Shen and Y. Yao, *Inorg. Chem.*, 2015, **54**, 4699–4708.
34 C. Kan, J. Ge and H. Ma, *Dalton Trans.*, 2016, **45**, 6682–6695.
35 G. Xiao, B. Yan, R. Ma, W. J. Jin, X. Q. Lu, L. Q. Ding, C. Zeng, L. L. Chen and F. Bao, *Polym. Chem.*, 2011, **2**, 659–664.
36 M. P. F. Pepels, M. Bouyahyi, A. Heisea and R. Duchateau, *Macromolecules*, 2013, **46**, 4324–4334.
37 K. S. Kwon, S. Nayab and J. H. Jeong, *Polyhedron*, 2015, **85**, 615–620.
38 N. W. Attandoh, S. O. Ojwach and O. Q. Munro, *Eur. J. Inorg. Chem.*, 2014, 3053–3064.
39 S. O. Ojwach, T. T. Okemwa, N. W. Attandoh and B. Omondi, *Dalton Trans.*, 2013, **42**, 10735–10745.
40 M. Zikode, S. O. Ojwach and M. P. Akerman, *Appl. Organomet. Chem.*, 2017, **31**, e3556.
41 M. Zikode, S. O. Ojwach and M. P. Akerman, *J. Mol. Catal. A: Chem.*, 2016, **413**, 24–31.
42 X. F. Yu, C. Zhang and Z. X. Wang, *Organometallics*, 2013, **32**, 3262–3268.
43 A. John, M. M. Shaikh, R. J. Butcher and P. Ghosh, *Dalton Trans.*, 2010, **39**, 7353–7363.
44 F. Xue, J. Zhao and T. S. A. Hor, *Dalton Trans.*, 2013, **42**, 5150–5158.
45 R. Mukherjee, *Coord. Chem. Rev.*, 2000, **203**, 151–218.
46 E. Ocansey, J. Darkwa and B. C. E. Makhubela, *RSC Adv.*, 2018, **8**, 13826–13834.
47 A. Budhai, B. Omondi, S. O. Ojwach, C. Obuah, E. Y. Osei-Twum and J. Darkwa, *Catal. Sci. Technol.*, 2013, **3**, 3130–3135.
48 Y. K. Kang, J. H. Jeong, N. Y. Lee, Y. T. Lee and H. Lee, *Polyhedron*, 2010, **29**, 2404–2408.
49 S. Shin, H. Cho, H. Lee, S. Nayab and Y. Kim, *J. Coord. Chem.*, 2018, **71**, 556–584.
50 S. Shin, S. Nayab and H. Lee, *Polyhedron*, 2018, **141**, 309–321.

51 H. Cho, S. Choe, D. Kim, H. Lee and S. Nayab, *Polyhedron*, 2020, **187**, 114641–114650.
52 I. Dvoretzky and G. H. Richter, *J. Org. Chem.*, 1950, **15**, 1285–1288.
53 F. Xue, J. Zhao and T. S. A. Hor, *Dalton Trans.*, 2011, **40**, 8935–8940.
54 S. Choi, Cobalt(II) and cadmium(II) complexes containing *N′*-substituted *N,N′,N*-bis((1H-pyrazol-1-yl)methyl)amine: Synthesis, structure and methyl methacrylate polymerization, *Thesis for the degree of Master of Science*, Kyungpook National University, 2014.
55 T. J. J. Whitehorne and F. Schaper, *Inorg. Chem.*, 2013, **52**, 13612–13622.
56 M. Cheng, A. B. Attygalle, E. B. Lobkovsky and G. W. Coates, *J. Am. Chem. Soc.*, 1999, **121**, 11583–11584.
57 B. M. Chamberlain, M. Cheng, D. R. Moore, T. M. Ovitt, E. B. Lobkovsky and G. W. Coates, *J. Am. Chem. Soc.*, 2001, **123**, 3229–3238.
58 M. T. Zell, B. E. Padden, A. J. Paterick, K. A. M. Thakur, R. T. Kean, M. A. Hillmyer and E. J. Munson, *Macromolecules*, 2002, **35**, 7700–7707.
59 J. W. Shin, K. Eom and D. Moon, *J. Synchrotron Radiat.*, 2016, **23**, 369–373.
60 Z. Otwinowski and W. Minor, *Methods Enzymol.*, 1997, **276**, 307–326.
61 G. M. Sheldrick, *Acta Crystallogr., Sect. A: Cryst. Phys., Diffr., Theor. Gen. Crystallogr.*, 2015, **71**, 3–8.
62 *SMART and SAINT-Plus v 6.22*, Bruker AXS Inc., Madison, Wisconsin, USA, 2000.
63 G. M. Sheldrick, *SADABS v 2.03*, University of Göttingen, Germany, 2002.
64 *SHELXTL v 6.10*, Bruker AXS Inc, Madison, Wisconsin, USA, 2000.
65 M. H. Sadhu and S. B. Kumar, *J. Mol. Struct.*, 2018, **15**, 239–247.
66 J. Seo, J. Lee, E. Kim, H. Lee, J. Jeon and S. Nayab, *Inorg. Chim. Acta*, 2019, **496**, 119071–119078.
67 M. E. Castro, M. J. Percino, V. M. Chapela, M. Ceron, G. Soriano-Moro, J. Lopez-Cruz and F. J. Melendez, *Int. J. Mol. Sci.*, 2013, **14**, 4005–4029.
68 E. Kim, H. Y. Woo, S. Kim, H. Lee, D. Kim and H. Lee, *Polyhedron*, 2012, **42**, 135–141.
69 S. Shin, S. H. Ahn, M. J. Jung, S. Nayab and H. Lee, *J. Coord. Chem.*, 2016, **69**, 2391–2402.
70 M. E. Kodadi, F. Malek, R. Touzani, A. Ramdani, S. E. Kadiri and D. Eddike, *Molecules*, 2003, **8**, 780–787.
71 A. W. Addison, T. N. Rao, J. Reedijk, J. van Rijn and G. C. Verschoor, *J. Chem. Soc., Dalton Trans.*, 1984, 1349–1356.
72 S. Toyota and M. Oki, *Bull. Chem. Soc. Jpn.*, 1992, **65**, 1832–1840.
73 H. Hopfl, *J. Organomet. Chem.*, 1999, **581**, 129–149.
74 J. Vela, J. Cirera, J. M. Smith, R. J. Lachicotte, C. J. Flaschenriem, S. Alvarez and P. L. Holland, *Inorg. Chem.*, 2007, **46**, 60–71.
75 D. Kim, S. Kim, H. Y. Woo, H.-J. Lee and H. Lee, *Appl. Organomet. Chem.*, 2014, **28**, 445–453.
76 L. Yang, D. R. Powell and R. P. Houser, *Dalton Trans.*, 2007, **9**, 955–964.
77 M. A. Masuelli, *J. Polym. Biopolym. Phys. Chem.*, 2014, **2**, 37–43.
78 I. Peckermann, A. Kapelski, T. P. Spaniol and J. Okuda, *Inorg. Chem.*, 2009, **48**, 5526–5534.
79 A. Stopper, T. Rosen, V. Venditto, I. Goldberg and M. Kol, *Chem.–Eur. J.*, 2017, **23**, 11540–11548.
80 S. Bian, S. Abbina, Z. Lu, E. Kolodka and G. Du, *Organometallics*, 2014, **33**, 2489–2495.
81 B.-H. Huang, C.-Y. Tsai, C.-T. Chen and B.-T. Ko, *Dalton Trans.*, 2016, **45**, 17557–17580.
82 L. Falivene, R. Credendino, A. Poater, A. Petta, L. Serra, R. Oliva, V. Scarano and L. Cavallo, *Organometallics*, 2016, **35**, 2286–2293. For online program, see https://www.molnac.unisa.it/OMtools/sambvca2.0/index.html.
83 Y. Cui, C. Chen, Y. Sun, J. Wu and X. Pan, *Inorg. Chem. Front.*, 2017, **4**, 261–269.
84 N. Ajellal, D. M. Lyubov, M. A. Sinenkov, G. K. Fukin, A. V. Cherkasov, C. M. Thomas, J.-F. Carpentier and A. A. Trifonov, *Chem.–Eur. J.*, 2008, **14**, 5440–5448.
85 M.-S. Kanga, J. Cho, S. Nayab and J. H. Jeong, *Polyhedron*, 2019, **158**, 135–143.
86 J. Lee, M. Yoon, H. Lee and S. Nayab, *RSC Adv.*, 2020, **10**, 16209–16220.
87 S. Nayab and J. H. Jeong, *Polyhedron*, 2013, **59**, 138–143.
88 U. Herber, K. Hegner, D. Wolters, R. Siris, K. Wrobel, A. Hoffmann, C. Lochenie, B. Weber and S. H. Pawlis, *Eur. J. Inorg. Chem.*, 2017, 1341–1354.
89 H. C. Pradhan, S. Mantri, A. Routaray, T. Maharaba and A. K. Sutar, *J. Chem. Sci.*, 2020, **132**, 25–31.
90 P. Marin, M. J.-L. Tschan, P. Haquette, T. Roisnel, I. del Rosal, L. Maron and C. M. Thomas, *Eur. Polym. J.*, 2019, **120**, 109208.
91 B. Rajashekhar and D. Chakraborty, *Polym. Bull.*, 2014, **71**, 2185–2203.
92 M. Mandal, U. Monkowius and D. Chakraborty, *J. Polym. Res.*, 2016, **23**, 1–9.
93 J. Lee, H. Lee, S. Nayab and K. B. Yoon, *Polyhedron*, 2019, **158**, 432–440.